Syntheses, structures, and magnetism of new vanadium and iron fluoride phosphates Ax(NH4)3-xM4(PO4)2F7(OH)2 (A=K, Rb, Cs , and M= V, Fe) containing novel structural motifs

Xinan Zhang, Yanling Jin, Wenxuan Zhu, Dan Chen, Qingqing Huang, Yaping Li, Olivier Mentré, Claire Minaud, Minfeng Lü

Title Page

Syntheses, structures, and magnetism of new vanadium and iron fluoride phosphates $A_x(NH_4)_{3-x}M_4(PO_4)_2F_7(OH)_2$ (A=K, Rb, Cs , and M= V, Fe) containing novel structural motifs

Xinan Zhang,[a] Yanling Jin, [a] Wenxuan Zhu,[a] Dan Chen, [a] Qingqing Huang,[a] Yaping Li, [a] Olivier Mentré,[b] Claire Minaud,[c] MinfengLü,[d]

[a] *School of Environmental & Chemical Engineering, Jiangsu University of Science and Technology, Zhenjiang 212100, Jiangsu, China*

[b]*Université Lille Nord de France, UMR 8181 CNRS, Unité de Catalyse et de Chimie du Solide (UCCS USTL), F-59655 Villeneuve d'Ascq, France.*

[c]*Univ. Lille, CNRS, INRAE, Centrale Lille, Univ. Artois, FR 2638 - IMEC - Institut Michel-Eugène Chevreul, F-59000 Lille, France.*

[d] *School of Materials Science and Engineering,, Jiangsu University of Science and Technology, Zhenjiang 212100, Jiangsu, China*

*Corresponding Author:

Professor Minfeng Lü

Fax: +86-511-85635850; Tel: +86-511-84401184; E-mail: m.f.lv@hotmail.com (M.F.Lu)

Graphical Abstract

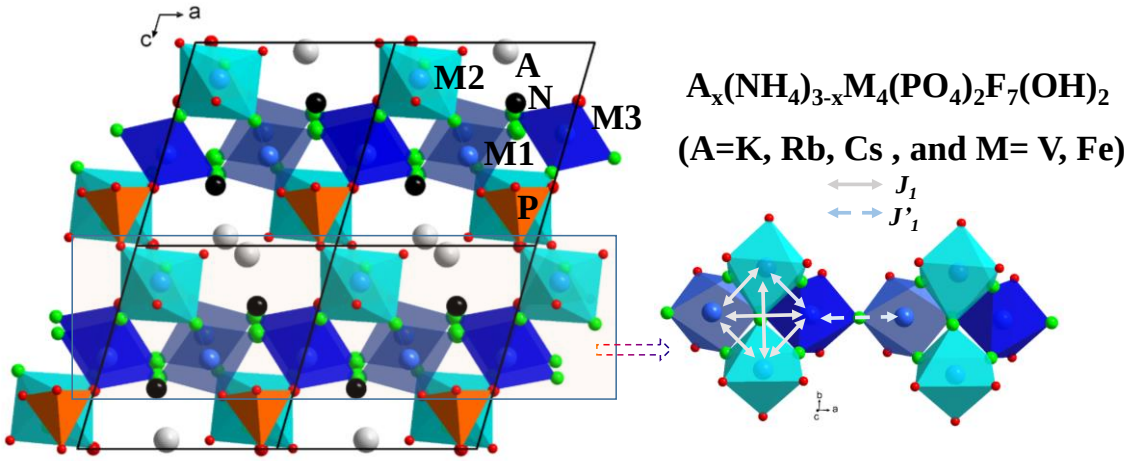

Graphical Table of Contents:

Three-dimensional frameworks of antiferromagnetic $A_x(NH_4)_{3-x}M_4(PO_4)_2F_7(OH)_2$ (A=K, Rb, Cs , and M= V, Fe) contains $_\infty[M_4O_8F_7(OH)_2]^{10-}$ chains formed by corner-shared cubane M_4 tetrahedron.

Highlights

Five new vanadium and iron fluoride phosphates $A_x(NH_4)_{3-x}M_4(PO_4)_2F_7(OH)_2$ (A=K, Rb, Cs , and M= V, Fe) were prepared through hydrothermal redox reactions.

Three-dimensional frameworks of $A_x(NH_4)_{3-x}M_4(PO_4)_2F_7(OH)_2$ (A=K, Rb, Cs , and M= V, Fe) contains $_\infty[M_4O_8F_7(OH)_2]^{10-}$ chains formed by corner-shared cubane M_4 tetrahedron.

All corner-shared cubane M_4 spin-chain (M= V^{3+}, Fe^{3+}) (S=1 or 5/2) exhibited antiferromagnetic interactions.

Abstract

Five new vanadium and iron fluoride phosphates $A_x(NH_4)_{3-x}M_4(PO_4)_2F_7(OH)_2$ (A=K, Rb, Cs , and M= V, Fe) were prepared through hydrothermal redox reactions. All compounds crystallize in the monoclinic crystal system, space group $P2_1/m$. The crystal structure constitutes three-dimensional frameworks with channels extending along [001] where A^+ or $(NH_4)^+$ ions reside in the channels. Novel structural motifs are made up of $_\infty[M_4O_8F_7(OH)_2]^{10-}$ chains formed by corner-shared cubane M_4 clusters. In the isostructural series, the interconnection between these units feature corner-shared cubane M_4 S = 1 spin-chains (M= V^{3+}) and corner-shared cubane M_4 S = 5/2 spin-chain (M= Fe^{3+}), which all promote antiferromagnetic (AFM) interactions.

Keywords: *transition metal oxide fluorides, building units, hydrothermal, single-crystal X-ray diffraction, magnetism,*

1. Introduction

Oxyfluoride groups, $M_xO_yF_z$ via the assembly with oxo-anions, such as $[BO_3]^{2-}$ $[CO_3]^{2-}$, $[PO_4]^{3-}$, and $[VO_4]^{3-}$ favor the formation of complex or unexplored structural types, often associated with low-dimensionality of the metallic sublattice [1]. From a structural standpoint, the fluorine atoms from $M_xO_yF_z$ groups reveal the combination of O and F electronegativities which gives versatile character to the central metals to their oxide counterparts [2], leading to new structures with unexpected complex edifices [1]. From a composition standpoint, the electronegative fluorine atom can effectively impacts the oxidation state of the central metal ion, which enhances the possibility of increasing complexity [3]. Thus, the rich structural chemistry of oxyfluorides has been exhibited a firm background for the discovery of novel structural motifs with unexpected properties [4].

Recently, fluoride phosphates have attracted particular attention due to their fascinating magnetic properties and quantum behavior. For example, $Na_3Cu_5(PO_4)_4F{\cdot}4H_2O$ with a Cu_5 cluster exhibits a broad maximum at 19.2 K, followed by a long-range AFM ordering at 11.5 K[5] due to 2D corrugated layer character. $Cu_2FePO_4F_4(H_2O)_4$ with a diamond chain composed of mixed-spins of Fe^{3+} (S = 5/2) and Cu^{2+} (S = 1/2 × 2) shows possible successive phase transitions with a noncollinear spin ordering [6]. $Ba_xFe_x(PO_4)F_y$ exhibits diverse magnetism: coupled spin-trimers in $Ba_3Fe_3(PO_4)F_{12}$ and *S* = 5/2 spin chain in $BaFe(PO_4)F_2$ [2].

We are interested in the combination of $[MO_xF_{6-y}]^{z+}$ units using $[PO_4]^{3-}$ ligands into original three-dimensional frameworks. Focusing on the synthesis of transition metal fluorophosphates, Fluoride-rich hydrothermal methods have proved to be a successful road, leading to a structurally diverse range of iron(III), manganese(III), cobalt(II), Nickel(II) and copper(II) fluorophosphates, comprised by $[PO_{4-m}F_m]^{n-}$(m=1,2.. n=2,1..) tetrahedral. However, this method is not efficient for the synthesis of transition metal fluoride phosphates, organized by unitary $[PO_4]^{3-}$ ligands. In order to obtain transition metal fluoride phosphates, transition metal fluorides are

obliged to work as a starting composition. We previously introduce hydrazine monohydrate to work as a reducing agent, followed by the formation of iron fluoride phosphates,i.e $Ba_3Fe_3(PO_4)F_{12}$.

In this context, we extend this method to first V(III) and novel Fe(III) analogs. The syntheses, structures, and magnetism of new vanadium and iron fluoride phosphates $A_x(NH_4)_{3-x}M_4(PO_4)_2F_7(OH)_2$ (A=K, Rb, Cs , and M= V, Fe) are reported.

2. Experimental section

2.1. Synthesis

Reagents. $FeCl_2{\cdot}4H_2O$ (Alfa Aesar, 98%), V_2O_5 (Energy Chemical, 99%), $KF{\cdot}2H_2O$(Sinopharm, 99%), RbF (Alfa Aesar, 99%), CsF (Energy Chemical, 99.5%), hydrazine monohydrate (Energy Chemical, 80 wt % in H_2O), H_3PO_4(Energy Chemical, 85% wt in H_2O), and HPF_6 (Alfa Aesar, 60% wt in H_2O) were used.

Synthesis. Single crystals were grown via hydrothermal reactions. Crystals of $(NH_4)_3V_4(PO_4)_2F_9$ (**I**) were grown in a mixture of 1.75mmol (0.3183g) of V_2O_5, 0.15 mL of H_3PO_4, 0.35 mL of HPF_6, 0.2mL of hydrazine monohydrate, and 2 mL of deionized water. Crystals of $Rb(NH_4)_2V_4(PO_4)_2F_9$ (**II**) were grown by combining 1.3125mmol (0.2387 g) of V_2O_5, 1.05 mmol (0.1097 g) of RbF, 0.75 mL of HPF_6, 0.2 mL of hydrazine monohydrate, and 2 mL of deionized water. Crystals of $Cs_{1.3}(NH_4)_{1.7}V_4(PO4)_2F_9$ (**III**) were grown in a mixture of 1.3125 mmol (0.2387 g) of V_2O_5, 1.75 mmol (0.2658 g) of CsF, 0.2mL of hydrazine monohydrate, and 2 mL of deionized water.Crystals of $K(NH_4)_2Fe_4(PO_4)_2F_9$ (**IV**) were grown by combining 2.8mmol(0.5566g) of $FeCl_2{\cdot}4H_2O$, 3.5mmol(0.3295g) of $KF{\cdot}2H_2O$, 0.104mL of H_3PO4, 0.5mL of HPF_6, 0.15mL of hydrazine monohydrate, and 1.52 mL of deionized water. Polycrystals of $Rb_{2.2}(NH_4)_{0.8}Fe_4(PO_4)_2F_9$ (**V**) were grown by combining 2.8mmol(0.5566g) of $FeCl_2{\cdot}4H_2O$, 5.6mmol(0.585g) of RbF, 0.104mL of H_3PO4, 0.5mL of HPF_6, 0.15mL of hydrazine monohydrate, and 1.52 mL of deionized water.

Each mixture was sealed into a 23 mL Teflon lined steel autoclave and heated to 220 °C for 72 h and then allowed to cool to room temperature slowly. Single crystals were recovered by washing them in an ultrasonic bath using anhydrous alcohol. Single-phase polycrystalline samples were obtained by grinding these single crystals for the measurements of their magnetic properties. Note that we failed to obtain big enough

single crystals of $Rb_{2.2}(NH_4)_{0.8}Fe_4(PO_4)_2F_7(OH)_2$for the single-crystal X-ray data collection.

2.2 X-ray Diffraction

Single-crystal X-ray data were collected at RT using a Bruker SMART APEX II diffractometer with a 1K CCD area detector and monochromated Mo Kα radiation (λ = 0.71073 Å). Integration of the obtained data were made using the program SAINT [7]. Absorption corrections were performed by the multi-scan method using the program SADABS [8] provided by the diffractometer manufacturer.

The crystallographic information is listed in Table 1.The detailed crystallographic data for all the reported compounds and the pertinent distances and angles are listed in Tables S1-S14. Deposition number CCDC 2247192, 2247193, 2247197, 2247198 for $(NH_4)_3V_4(PO_4)_2F_9$, $Rb(NH_4)_2V_4(PO_4)_2F_9$, $Cs_{1.3}(NH_4)_{1.7}V_4(PO4)_2F_9$, $K(NH_4)_2Fe_4(PO_4)_2F_9$ respectively.

For product purity, powder X-ray diffraction data were collected using a Bruker D8 Advance X-ray powder diffractometer with a normal scan with a step size of 0.04◦ and a counting time of 0.5 s per step was performed. The XRD powder patterns shown in Figure S1-S4, match well with the calculated patterns using the single crystal models. For $Rb_{2.2}(NH_4)_{0.8}Fe_4(PO_4)_2F_7(OH)_2$, the diffraction pattern using a step scan mode with a step size of 0.025◦ and a counting time of 2 s per step in the range 2θ 15–115◦was adopted. The unit cell of $Rb_{2.2}(NH_4)_{0.8}Fe_4(PO_4)_2F_7(OH)_2$ was first determined from the X-ray powder diffraction patterns using indexing programs DICVOL91 [9] based on the first 50 lines for the search of solutions. Subsequent Rietveld refinements (Figure S5) with a starting model of the crystal data for $K(NH_4)_2Fe_4(PO_4)_2F_7(OH)_2$ in the space group $P\ 2_1/m$ were performed with the program Jana2006[10] after a profile matching step, introduced by Le Bail et al. [11].

2.3. Energy dispersive analysis by X-ray/Scanning electron microscopy (EDX/SEM)

Qualitative EDX analyses were carried out using a Phenom ProX desktop analyser. EDX analyses (Figure S6-S10) for $(NH_4)_3V_4(PO_4)_2F_7(OH)_2$, $Rb(NH_4)_2V_4(PO_4)_2F_7(OH)_2$, $Cs_{1.3}(NH_4)_{1.7}V_4(PO_4)_2F_7(OH)_2$ $K(NH_4)_2Fe_4(PO_4)_2F_7(OH)_2$ and $Rb_{2.2}(NH_4)_{0.8}Fe_4(PO_4)_2F_7(OH)_2$, exhibited approximate A:M:P:F ratios of 0:3.52:2:7.2, 1:.3.45:1.91:7.79,1.25:3.4:2.0:8.22, 1:3.44: 1.96:7.95 and 1.75:4: 1.85:6.69, respectively.

2.4. Infrared spectroscopy

Infrared spectra for the reported materials were recorded on an Agilent Cary 670-IR FTIR spectrometer with an attenuated total reflection (ATR) accessory in the range of 400−4000 cm^{-1}. Figure S11-S12 shows the FTIR spectra of the title compounds. Apart from weak broad absorption bands in the range of 3040–3260 cm^{-1}which can be assigned to the $v_3(NH_4^+)$ region [12] (may be overlapped with O–H^- stretching vibrations at this region), two groups of bands originating from $[PO_4]^{3-}$ vibrations can be distinguished: The vibrational band found in the range of 1080–1000 cm^{-1}， due to stretching vibrations of P–O phosphate group[13]. The lower strong doublet, compared with typically 1120 cm^{-1} of $V_{as}[PO_3F]^{2-}$ asymmetric mode and 1010 cm^{-1} $V_s[PO3F]^{2-}$ symmetric mode, further confirm the presence of $[PO_4]^{3-}$ groups[14,15], only. The bands at 670–400 cm^{-1} originates from O–P–O bending vibrations[13].

2.5.Magnetic measurements.

Magnetic susceptibility were investigated using a vibrating sample magnetometer (VSM-SQUID, Quantum Design, PPMS). magnetic susceptibilities were measured in the temperature range of T=2 – 400 K under an applied field of H= 0.1 T using Zero-field-cooled (ZFC) and field-cooled (FC) experiments. Isothermal magnetization curves were obtained at different temperature by sweeping the external magnetic field from -9T to 9 T.

3. Results and discussion

All reported compounds crystallized in the monoclinic crystal system with space

group of space group $P2_1/m$. The crystal structures were solved using a charge-flipping program [16] and refined by full-matrix least-squares on F^2 via the Jana 2006 program [10]. The fluorine atoms were determined by local difference Fourier map techniques and the bond valence sum (BVS) calculation [17], which were used the similar process and partly reported elsewhere [2,18,19]. The hydrogen atoms around the ammonium cations and oxygen anions were determined by difference Fourier maps and constrained on the basis of geometric criteria [20]. The crystallographic information is given in Table 1. It should be mentioned that the assignment of F atoms is reasonable for narrow space impede the occupation of H^+, which will produce the electrostatic repulsion between H^+ specis and M^{3+} cations. However, there may be a slight disordering on the O(1) site with mixed O/F occupancy For the sake of simplicity, we preclude the possibility of slight partial occupancy of F atoms. Finally, the reasonable formula with $A_x(NH_4)_{3-x}M_4(PO_4)_2F_7(OH)_2$ (A=K, Rb, Cs , and M= Fe, V) were confirmed with bond valence sum calculations [17] for the cations V^{3+}, Fe^{3+} and P^{5+} and anions O^{2-} and F^- of 3.12(2)-3.22(2),3.05(2)-3.33(1), 5.04(5)-5.08(4), 1.61(1)-1.99(1) and 0.88(1)-1.06(1), respectively, as summarized in Table 2.

All isostructural compounds reveal thesimilar crystal structures, whose unit cell parameters for V and Fe compounds are listed in Table 1. The expansion of the unit cell volume is observed, for which a relatively larger volume cation is accompanied by a larger A sites, in accordance with Vegard's law.

The macroanionic framework of $A_x(NH_4)_{3-x}M_4(PO_4)_2F_7(OH)_2$ (A=K, Rb, Cs , and M= Fe, V) consists of heteroleptic *cis*-$M(1)F_4O_2$, *cis*-$M(3)F_4O_2$ octahedra, *facial*-$M(2)F_3O_2(OH)$ octahedra and PO_4 tetrahedra. Typical coordinates are given in Fe compounds, for instance, $K(NH_4)_2Fe_4(PO_4)_2F_7(OH)_2$ as is shown in Figure 1. The Fe(1) and Fe(3) are located on a mirror plane (Wyckoff position 2*e*), which both feature a slightly distorted octahedral coordination. The Fe(1) connected with four F atoms with bond lengths in the range of 1.944(7)-1.958(4) Å, and coordinated to two O atoms with the equidistant bond lengths of 1.963(5) Å with F /O−Fe(1)− F/O bond angles of

84.72(19)- 95.8(2)°(see Table S12). In the more distorted *cis*-[Fe(3)F_4O_2] unit, Fe(3)−F distances are between 1.941(6) and 1.967(5) Å, while the equidistant Fe(3)−O bond distances are 1.933(5) Å with O/F−Fe(3)−O/F bond angles of 84.74(19)- 98.4(2)°. The Fe(2) cations located on a general position (Wyckoff position 4*f*), which are surrounded by three F atoms and three O atoms in distorted facial-M(2)F_3O_2(OH) geometry with the mean Fe-F bond distance of 1.991(5) Å and Fe-O bond distance of 1.924(5), leading the F /O−Fe(1)− F/O bond angles of 83.59(18)- 95.2(2)°. The unique P(1) forms a distorted PO_4^{3-} groups , with the P-O bond lengths ranging from 1.525(6) to 1.536(5) Å.

The linear $_\infty[Fe_2F_6O_4]^{10-}$ moieties formed by fluorine corner shared alternating Fe(1)F_4O_2 and Fe(3)F_4O_2 octahedra that are connected by Fe(2)F_3O_2(OH) octahedra at intervals through fluorine ligands (see Figure 2a). More simply, cubane Fe_4 units are connected with each other to form through corner-shared fluorine ligands to form a linear $_\infty[M_4O_8F_7(OH)_2]^{10-}$ chain.Two Fe(2)F_3O_2(OH) octahedra and two Fe(3)F_4O_2 octahedra are linked with two PO_4 tetrahedra through fluorine /oxide ligands, leading to an six-membered ring (6-MR) (see Figure 2b), where 4-,5-, and 6-MR channels extend along the [100] direction. While the connection of two Fe(1)F_4O_2 octahedra, two Fe(2)F_3O_2(OH) octahedral and two Fe(3)F_4O_2 octahedra with two PO_4 tetrahedra through oxide/ fluorine ligands leading to 8-MRs along the [010] direction (see Figure 2c). The crystal structure of $A_x(NH_4)_{3-x}M_4(PO_4)_2F_7(OH)_2$ (A=K, Rb, Cs , and M= Fe, V) is thus built from 3D transition metal framework where A^+ or $(NH_4)^+$ cations reside in the 8-MR channels frameworks. The framework may be described as a linear $_\infty[M_4O_8F_7(OH)_2]^{10-}$ chain (see Figure 2a,2b) formed by cubane tetranuclear clusters $[M_4O_8F_7(OH)_2]^{10-}$ via corner-sharing fluorine atoms, which featured a slightly distorted tetrahedral cage structure with *Cs* symmetry (see Figure 2a,2b) along the *a* directions, isolated by PO_4 groups.

We examined the local cubane M_4 tetrahedron structures in detail and compared

them together. All the all V compounds possess a longer M-M distances than those in Fe compounds along the chain. The average V1−V3 and V3−V1 distances range from 3.577(1) Å to 3.601(3) Å, while the average Fe1−Fe3 and Fe3−Fe1 distances is 3.55(1) Å. The deviation of M-F-M bond angles around fluorine ligands along the chain are 8.8-10°for V series and12.4° for **IV** respectively.

Inside cubane M_4 tetrahedron, vertical to the chain, enhancing M2-M2 distance companied with enhancing ∠M2-F5-M2 is observed in Fe series. In **IV**, the Fe2−Fe2 distance is 3.781(2) Å, and Fe2−F5-Fe2 bond angles is 147.1(3)^o, respectively, compared to Fe2−Fe distance of 3.84(1) Å and the Fe2−F5-Fe2 bond angles of 148.7(2)^o in **V**. However, there is no regulation about the connection between two M2 atoms and one M1 and M3 atoms. It is the structural distortion that is the manifestation of accommodation of different A-sites cations.

Figure 4a, 4c exhibits the temperature dependence of $\chi(T)$ for $A_x(NH_4)_{3-x}V_4(PO_4)_2F_7(OH)_2$ (A= Rb, Cs) under an applied field of 1 kOe during ZFC processes. Note that the ZFC and FC data do not diverge, which rules out the presence of a net residual magnetic moment. Similar magnetic behaviors were found in the V compounds , thus, only the detailed magnetic analysis of $Rb(NH_4)_2V_4(PO_4)_2F_7(OH)_2$ is provided below. $\chi(T)$ displayed a steep increase when the temperature decreased. The inverse susceptibility data however showed two regimes in the whole range of the temperature, as shown in Figure S13. Curie–Weiss analysis of $1/\chi(T)$ vs. T for $Rb(NH_4)_2V_4(PO_4)_2F_7(OH)_2$ (**II)** was fitted to an effective magnetic moment of μ_{eff}=2.65(2) μ_B per V^{3+} and the Curie–Weiss temperature θ_{CW}=-29(1) K between 30 K and 400 K. The calculated value of μ_{eff} is very close to the spin-only value of 2.76 μB for S=1 V^{3+} ions. The negative Weiss constant of θ_{CW} suggests predominant AFM interactions. The effective magnetic moment and Weiss temperatures (θ_{CW}) for each sample are listed in Table 3.

We further analyzed the high-temperature $\chi(T)$, first by considering the magnetic susceptibility amongst interacting $(V^{3+})_4$ subunits discussed above. For simplification

reasons, we assume that all exchanges inside the tetranuclear units (3 distinct in total) are equivalent and labelled J_1.

According to geometrical considerations, two reasonable exchanges J_1 and J'_1 were considered, as shown in Figure 3. J_1 and J'_1 superexchange path involves V-F-V exchanges inside and outside of M_4 tetrahedron, which can be expected to be strong. Note that V-F-F-Vsuper-super-exchange interactions along the chains, and V-O-O-V super-super-exchange interactions across the chains can be assumed to be weak [21,22], which thus are neglected for the simplicity.

Then the magnetic susceptibility of ideal pyrochlore-like tetrahedral clusters (χ_{tet}) was analyzed for various spin values in ref 23. For S=1, the analytical expression is:

$$\chi_{\text{tet}}(T) = \frac{4Ng^2\beta^2}{k_B T} \frac{x^2 + 5x^6 + 7x^{12} + 5x^{20}}{1 + 6x^2 + 10x^6 + 7x^{12} + 3x^{20}}$$

with $x = \exp(J_1/T)$.

The magnetic susceptibility of each ion in the tetranuclear units is written as

$$\hat{\chi_{tet}}(T) = \chi_{\text{tet}}(T)/4$$

In order to estimated the interaction between the V_4 tetranuclears, a modified mean-field model can be established by

$$\chi_{\text{intra}}(T) = \frac{\hat{\chi_{tet}}(T)}{1 - \frac{2zJ'_1}{Ng^2\beta^2}\hat{\chi_{tet}}(T)} + \chi_o,$$

Where J'_1 is V-F-V super-interactions beyond the V_4 tetranuclears, Z=0.5 for half ions in the tetranuclear interact with one external ion. Furthermore, χ_o corresponds to diamagnetic components and the temperature-independent susceptibility of the Van Vleck orbital.

We further assume $J'_1 = J_1$ for J'_1 and J_1 superexchange interactions are mediated by similar V-F-V angles and V-V distance. The fitting for $\chi(T)$ yields g=1.76(3), J_1/k_B=-4.1(2) K, and χ_o=0.00002(1) emu·mol^{-1}·Oe^{-1} (R^2 =0.9996). It should be noted that the model cannot fit the magnetic susceptibility below 40 K due to the frustration [21]. Compared with the model of ref 23, where frustration has been taken into account and $\chi(T)$ upturn at low temperate is able to reproduce. The current results are due to the

approximations between and inside tetranuclears. In this case, the introduction of paramagnetic fraction would be more realistic.

Isothermal magnetization curve M(H) was measured at different temperature, as shown in Figure 4b. *M*(H) shows a linear increase when the magnetic field increases at T≥30K thanks to the presence of AFM interactions. However, At T=2K, M(H) increases rather steeply with increasing field up to 1.0 T and then gradually curves up, with no hysteresis behavior between the up and the down sweep. At H = 9 T, the magnetization approaches the saturated value of ~2 μB/f.u. The magnetization curve has pronounced deviations from Brillouin function indicative for rather robust frustrated AFM.

Figure 5a, 5c shows the plots of $\chi(T)$ with respect to T of $A_x(NH_4)_{3-}Fe_4(PO_4)_2F_7(OH)_2$ (A=K, Rb). Similar magnetic behaviors were found, thus, only the detailed magnetic analysis of $K(NH_4)_2Fe_4(PO_4)_2F_7(OH)_2$ is provided here. Detailed results from Analysis of dc magnetic susceptibility are summarized in Table 3.From $d\chi T(T)/d\ T$ versus T, a small peak at T_N = 5.5 K can be identified. We derive a Curie−Weiss temperature of the effective magnetic moment μ_{eff}= 5.62 μ_B, which is comparable to the theoretical spin-only value of 5.92 μ_B for the S=5/2 state and Curie-Weiss temperature θ_{CW}= -277(1) K at high temperatures of 50-400K. The large value of θ_{CW} is indicative of AFM couplings in **IV**.

The magnetic data of **IV** were fitted using the simplified model described in the reference 21.The extracted magnetic parameters are g=1.99(2), J_1/k_B=-11.2(2) K, and χ_o=0.000006(2) emu·mol^{-1}·Oe^{-1} (R^2 =0.9962). We note that J_1 is quite close those in tetranuclear Fe(III) chains [21]. Finally, The $M(H)$ data at different temperature show a linear increase from −9 T to 9 *T*, in agreement with the AFM state (Figure 5b).

4. Conclusions

We have hydrothermally synthesized five vanadium and iron fluoride phosphates $A_x(NH_4)_{3-x}M_4(PO_4)_2F_7(OH)_2$ (A=K, Rb, Cs , and M= V, Fe), stemming from

fluorophosphoric and phosphoric acids as a fluorine source, and hydrazine monohydrate working as a reducing agent. $A_x(NH_4)_{3-x}M_4(PO_4)_2F_7(OH)_2$ reveal three-dimensional (3D) frameworks containing novel structural motifs of $_\infty[M_4O_8F_7(OH)_2]^{10-}$ chains formed by corner-shared cubane tetranuclear clusters $_\infty[M_4O_8F_7(OH)_2]^{10-}$ chains. The isostructural two series feature corner-shared cubane M_4 S = 1 spin-chain (M= V) and corner-shared cubane M_4 S = 5/2 spin-chain (M= Fe), which all promote AFM interactions.

5. Supplementary material

Calculated and observed X-ray diffraction patterns, infrared spectra, EDX data, and detailed crystallographic data for all the reported materials are available (PDF).

AUTHOR INFORMATION

Corresponding Author

m.f.lv@hotmail.com (Minfeng Lü)

ORCID[ID]
Minfeng Lü: 0000-0003-2576-3840

Notes

The authors declare no competing financial interests.

Acknowledgments

This work was financially supported by the National Natural Science Foundation of China (21671185).

References

[1] J.A. Armstrong, E.R. Williams, M.T. Weller, Fluoride-Rich. J. Am. Chem. Soc. (133) 2011 8252.

[2] J. Jiang, S. Lee, B. Zhu, Y. Yu, J. C. Waerenborgh, K.-Y. Choi, M. Lü. Inorg. Chem. (58) 2019 133.

[3] J. Yeon, J. B. Felder, M.D. Smith, G. Morrison and H.-C. zur Loye CrystEngComm (17) 2015 8428.

[4]H. Kageyama, K. Hayashi, K. Maeda, J. P. Attfield, Z. Hiroi, J. M. Rondinelli, K. R. Poeppelmeier, Nat. Commun. (9) 2018 772.

[5]X.Y.Yue, Z.W. Ouyang, M.Y. Cui, L.Yin, G. L.Xiao, Z.X.Wang, J.Liu, J.F.Wang, Z.C.Xia, X.Y.Huang, Z. Z. He. Inorg. Chem. (57) 2018 3151.

[6]H.Lu, N. Hayashi, Y.Matsumoto, H.Takatsu, H.Kageyama, Inorg. Chem. (56) 2017 9353.

[7] SAINT, Area-Detector Integration Software, Siemens Industrial Automation. Inc. Madison. 1996.

[8] SADABS, Area-Detector Absorption Correction, Siemens Industrial Automation. Inc. Madison. 1995.

[9] D. Louer, M. Louer, J. Appl. Cryst. 5 (1972) 271; A. Boultif, D. Louer, J. Appl. Cryst. 24 (1991) 987.

[10] V. Petricek, M. Dusek and L. Palatinus. Jana2006. The crystallographic computing system. Institute of Physics. Praha. Czech Republic. 2006.

[11] A. Le Bail, H. Duroy, J.L. Fourquet, Mater. Res. Bull. 23 (1988) 447.

[12]D.D. Weis, G. E. Ewing J. Geophys. Res. (101) 1996 709.

[13]W. Jastrzębski, M. Sitarz, M. Rokita, K. Bułat Spectrochim. Acta A 79 (2011) 722.

[14]B. Zhu, J. Jiang, T. Zhu, H. Yang, Y. Jin, K.-Y. Choi, M. Lu, Inorg. Chem. (59) 2020 3794.

[15]M.Weil, E. J. Baran, R. K. Kremer, E.Libowitzky, Z. Anorg. Allg.Chem. (641) 2015 184.

[16] L. Palatinus and G. Chapuis. J. Appl. Crystallogr. (40) 2007 786.

[17] N.E. Brese and M.O' Keeffe. Acta Crystallogr. (B47) 1991 192.

[18] J. Jiang, B. Zhu, T. Zhu, H. Yang, Y. Jin, M. Lü. Dalton. Trans. (49) 2020 841.

[19]M. Lü, J. Jiang, B. Zhu, Y. Zhao, T. Zhu, H. Yang, Y. Jin, H. Kabbour, K.-Y. Choi, W. T. A. Harrison. Dalton Trans. (49) 2020 2234.

[20] R.B. Helmholdt, G.A. Wiegers and J. Bartolomé. Journal of Physics C: Solid State Physics. (13) 1980 5081.

[22] Y. Jin, S.Lee, T. Zhu, X. Zhang, H. Yang, D. Chen, W. Zhu,K.-Y. Choi, M. Lu Inorg. Chem. (61) 2022 9257.

[22] H. B. Yahia, E. Gaudin, J. Darriet, M. Banks, R. K. Kremer, A. Villesuzanne, M.-H. Whangbo,Inorg. Chem. (44) 2005 3087.

[23] A. J.García–Adeva, D. L. Huber Phys. Rev. Lett. (85) 2000 4598.

Figure Captions

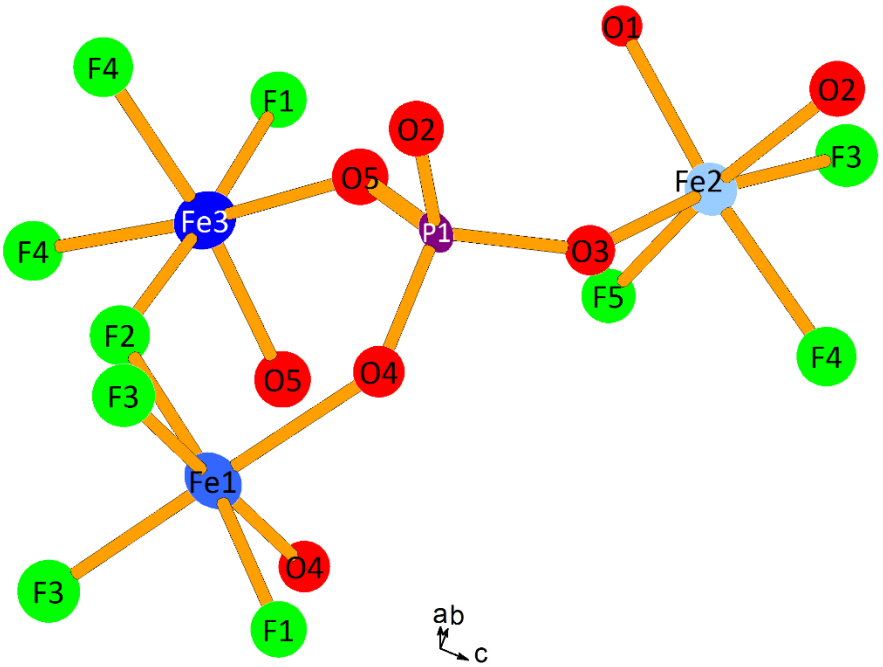

Fig. 1 Coordination geometry of the Fe and P cations by O/F atoms for $K(NH_4)_2Fe_4(PO_4)_2F_7(OH)_2$. H^+ species have been removed for clarification.

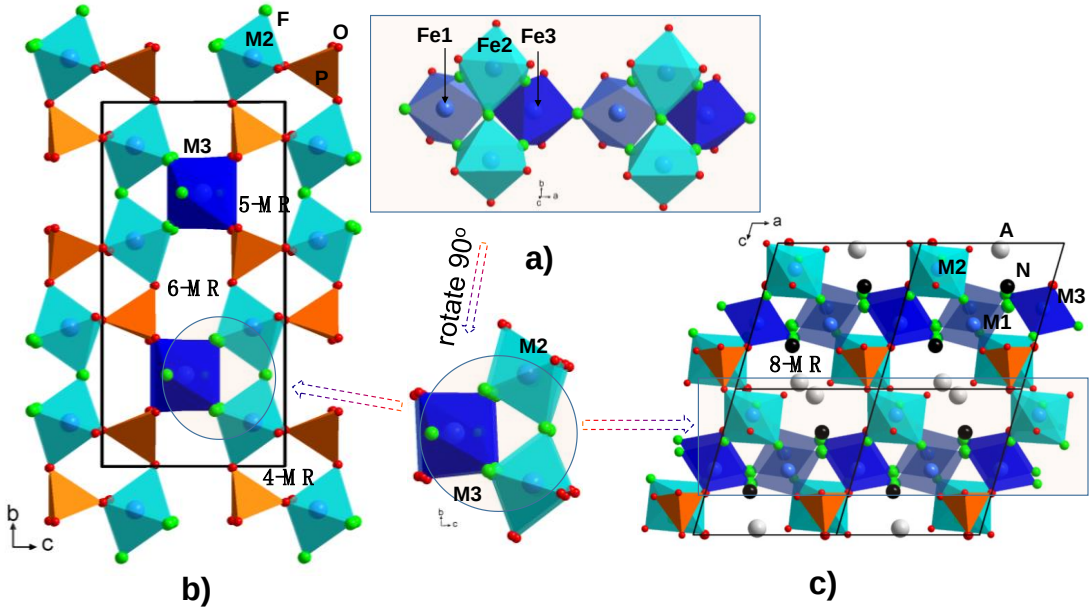

Fig. 2 (a) Projection of a linear $_\infty[M_4O_8F_7(OH)_2]^{10-}$ chain in $A_x(NH_4)_{3-x}M_4(PO_4)_2F_7(OH)_2$ (A=K, Rb, Cs , and M= V, Fe) along the *a*-axis and the slightly slit *c*-axis. Isostructual $K(NH_4)_2Fe_4(PO_4)_2F_7(OH)_2$ is exemplified, whereas *cis*-$M(1)F_4O_2$ and *cis*-$M(3)F_4O_2$ octahedra is drawn in light blue,dark blue,respecitively, and *facial*-$M(2)F_3O_2(OH)$ octahedral is highlighted in light cyan. PO_4 groups are drawn in orange. (b) Projection of the structure of $A_x(NH_4)_{3-x}M_4(PO_4)_2F_7(OH)_2$ (A=K, Rb, Cs , and M=

V, Fe) along the *a*-axis. A^+ cations and NH_4^+ groups have been removed for clarification.

(c) Projection of the structure of $A_x(NH_4)_{3-x}M_4(PO_4)_2F_7(OH)_2$ (A=K, Rb, Cs , and M= V, Fe) along the *b*-axis. H^+ species have been removed for clarification.

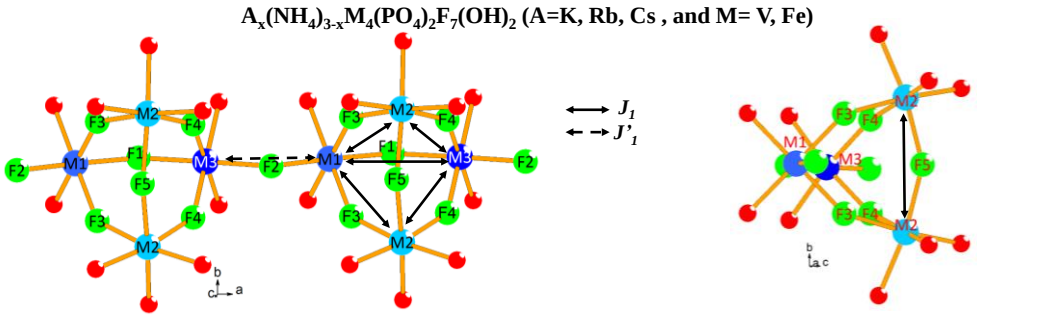

I ∠ V1-F1-V3= 135.95(19) º ∠ V1-F2-V3= 127.2(2) º ∠ V1-F3-V2= 145.2(2) º ∠ V2-F4-V3 = 143.5(2) º ∠V2-F5-V2= 143.3(2) º
V1-V3=3.655(2)Å, V3-V1=3.523(2)Å, V1-V2=3.759(1)Å, V2-V3=3.770(1)Å, V2-V2=3.736(1)Å

II ∠ V1-F1-V3= 136.3(4) º ∠ V1-F2-V3= 126.4(4) º ∠ V1-F3-V2= 145.7(3) º ∠ V2-F4-V3 = 144.2(3) º ∠V2-F5-V2= 144.1(4)º
V1-V3=3.651(4)Å, V3-V1=3.502(4)Å , V1-V2=3.766(2)Å, V2-V3=3.776(3)Å, V2-V2=3.740(2)Å

III ∠ V1-F1-V3= 136.9(4) º ∠ V1-F2-V3= 127.0(4) º ∠ V1-F3-V2= 144.7(2) º ∠ V2-F4-V3 = 143.8(2) º ∠V2-F5-V2= 145.4(4)º
V1-V3=3.667(3)Å, V3-V1=3.534(3)Å , V1-V2=3.776(2)Å, V2-V3=3.787(3)Å, V2-V2=3.724(2)Å

IV ∠ Fe1-F1-Fe3=138.0(3) º ∠ Fe1-F2-Fe3=125.6(3) º ∠ Fe1-F3-Fe2=143.9(2) º ∠ Fe2-F4-Fe3 =145.0(2) º ∠Fe2-F5-Fe2=147.1(3)º
Fe1-Fe3=3.627(2)Å, Fe3-Fe1=3.474(2)Å, Fe1-Fe2=3.768(1)Å, Fe2-Fe3=3.778(2)Å, Fe2-Fe2=3.781(2)Å

V ∠ Fe1-F1-Fe3= 132.7(13) º ∠ Fe1-F2-Fe3= 131.8(17) º ∠ Fe1-F3-Fe2= 142.6(12) º ∠ Fe2-F4-Fe3 = 143.3(13) º ∠Fe2-F5-Fe2= 148.7(18)º
Fe1-Fe3=3.55(1)Å, Fe3-Fe1=3.55(2)Å, Fe1-Fe2=3.77(1)Å, Fe2-Fe3=3.79(1)Å, Fe2-Fe2=3.84(1)Å

Fig. 3 Comparison of the M^{3+} tetrahedral cage unit of $A_x(NH_4)_{3-x}M_4(PO_4)_2F_7(OH)_2$ (A=K, Rb, Cs , and M= V, Fe). The M−F−M bond angles and M−M cations distances are summarized.

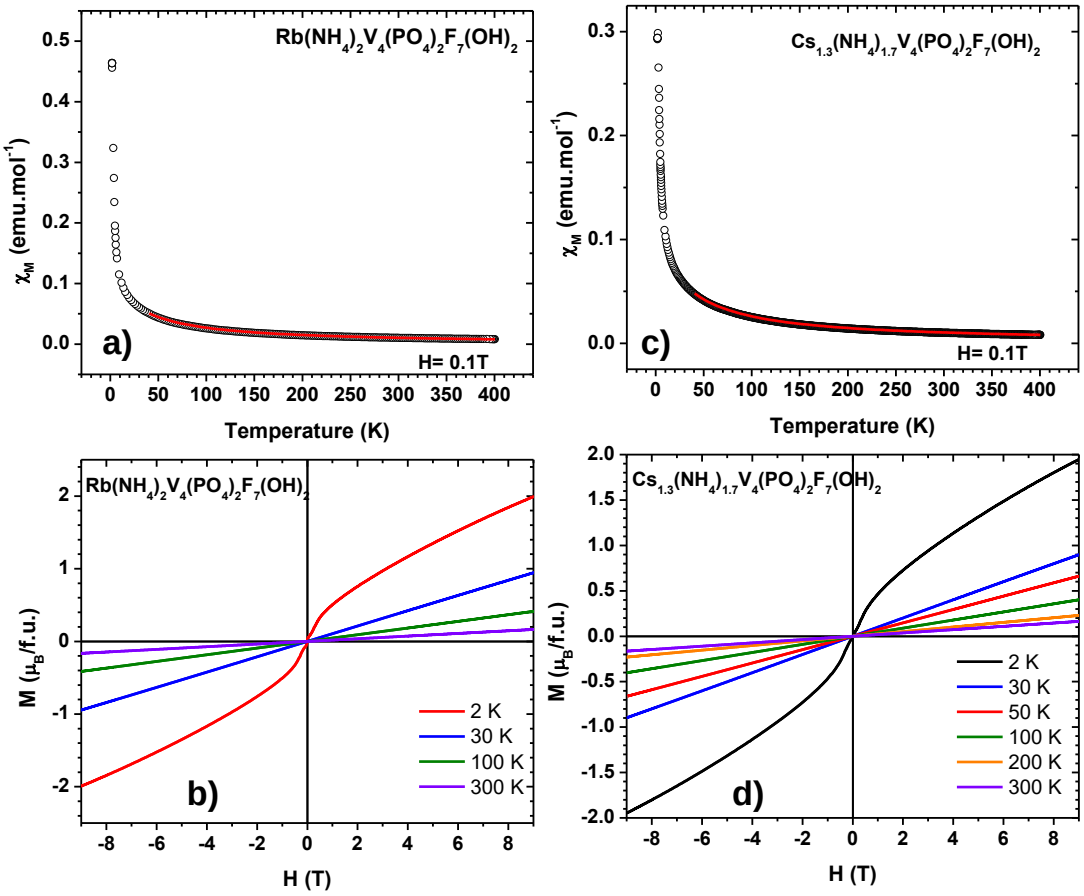

Fig. 4 a) and c) Experimental χ(T)/T for the V compounds in an applied magnetic field of 0.1T.The solid line corresponds to the fit to the data above 40 K. b) and d) Isothermal magnetization collected at different temperature.

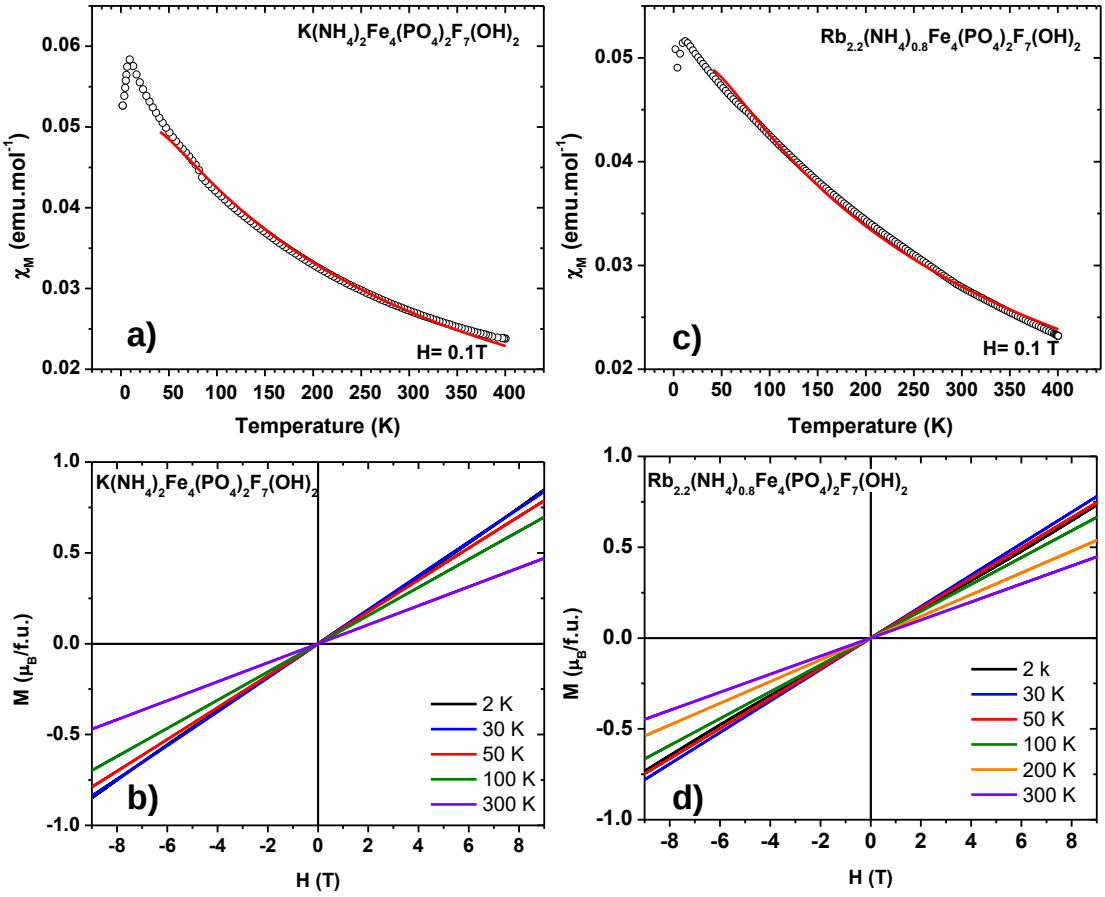

Fig. 5 a) and c) Experimental χ(T)/T for the Fe compounds in an applied magnetic field of 0.1T. The solid line corresponds to the fit to the data above 40 K. b) and d) Isothermal magnetization collected at different temperature.

Table 1. Crystal data, structure solutions and refinements for $A_x(NH_4)_{3-x}M_4(PO_4)_2F_7(OH)_2$ (A=K, Rb, Cs , and M= V, Fe) at room temperature.

	$(NH_4)_3V_4(PO_4)_2F_7(OH)_2$	$Rb(NH_4)_2V_4(PO_4)_2F_7(OH)_2$	$Cs_{1.3}(NH_4)_{1.7}V_4(PO_4)_2F_7(OH)_2$	$K(NH_4)_2Fe_4(PO_4)_2F_7(OH)_2$	$Rb_{2.2}(NH_4)_{0.8}Fe_4(PO_4)_2F_7(OH)_2$
Molar weight	614.8	682.2	764.1	655.5	779.6
Symmetry	monoclinic	monoclinic	monoclinic	monoclinic	monoclinic
Space group	*P 2₁/m*	*P 2₁/m*	*P 2₁/m*	*P 2₁/m*	*P 2₁/m*
Z	2	2	2	2	2
a (Å)	7.1770(2)	7.1520(14)	7.2090(2)	7.0999(4)	7.1078(4)
b(Å)	14. 4431(4)	14.445(3)	14.4711(3)	14.4640(8)	14.4253(9)
c (Å)	7.5652(2)	7.5841(14)	7.6567(2)	7.5364(4)	7.5903(5)
β (°)	106.750(2)	106.517(14)	106.694(2)	106.161(1)	106.334(3)
V ($Å^3$)	750.92(4)	751.2(2)	765.10(3)	743.35(7)	746.84(8)
T(K)	293	293	293	293	293
μ (mm^{-1})	2.763	5.977	5.756	4.456	
R(int) (%)	5.6	9.74	6.01	3.2	
indep all (I >	1939	1927	1971	1919	
indepobsd (I >	1461	993	1362	1672	
Number of refined	75	75	80	75	71
R(F)[a] [*I* >3σ(*I*)/all	4.44/6.52	6.98/14.79	5.09/7.79	6.14/6.99	8.29/8.46
R_w (F^2)[b] [*I*	4.83/5.02	6.88/7.62	6.14/6.40	9.94/9.92	8.34/8.36
Max/Min residual	1.21/-0.45	3.22/-1.41	1.48/-1.36	2.12/-2.41	1.09/-3.23

[a] $R = \sum \| F_o| - |F_o \| / \sum |F_o|$, [b] $R_w = [\sum w(|F_o^2| - |F_c^2|)^2 / \sum w|F_o^2|^2]^{1/2}$]

[b] *Results from X-ray Rietveld refinement*

Table 2. Bond valence sum (BVS) of $A_x(NH_4)_{3-x}M_4(PO_4)_2F_7(OH)_2$ (A=K, Rb, Cs , and M= V, Fe).

$(NH_4)_3V_4(PO_4)_2F_7(OH)_2$			$Rb(NH_4)_2V_4(PO_4)_2F_7(OH)_2$				$Cs_{1.3}(NH_4)_{1.7}V_4(PO_4)_2F_7(OH)_2$				$K(NH_4)_2Fe_4(PO_4)_2F_7(OH)_2$				$Rb_{2.2}(NH_4)_{0.8}Fe_4(PO_4)_2F_7(OH)_2$			
Atom	**V_V^c**	**V_P^c**	**Atom**	**V_{Rb}^c**	**V_V^c**	**V_P^c**	**Atom**	**V_{Cs}^c**	**V_V^c**	**V_P^c**	**Atom**	**V_K^c**	**V_{Fe}^c**	**V_P^c**	**Atom**	**V_{Rb}^c**	**V_{Fe}^c**	**V_P^c**
V1	3.18(1)		Rb1	0.95(1)			Cs1	1.29(1)			K1	0.92(1)			Rb1	1.35(2)		
V2	3.14(1)		Rb2	1.23(1)			Cs2	1.81(1)			Fe1		3.05(2)		Rb2	0.97(2)		
V3	3.17(1)		V1		3.22(2)		V1		3.12(2)		Fe2		3.22(2)		Fe1		2.95(8)	
P1		5.04(2)	V2		3.17(2)		V2		3.12(2)		Fe3		3.14(2)		Fe2		3.31(6)	
			V3		3.17(2)		V3		3.19(2)		P1			5.08(4)	Fe3		3.16(9)	
			P1			5.04(5)	P1			5.07(4)					P1			4.8(2)
Atom	**V_F**	**V_O**	**Atom**	**V_F**	**V_O**		**Atom**	**V_F**	**V_O**		**Atom**	**V_F**	**V_O**		**Atom**	**V_F**	**V_O**	
F1	-0.98(1)		F1	-1.01(1)			F1	-1.00(1)			F1	-1.04(1)			F1	-1.10(4)		
F2	-0.98(1)		F2	-1.05(2)			F2	-1.00(1)			F2	-1.06(1)			F2	-1.06(5)		
F3	-0.93(1)		F3	-1.01(1)			F3	-0.99(1)			F3	-0.88(1)			F3	-0.94(4)		
F4	-0.97(1)		F4	-0.96(1)			F4	-1.02(1)			F4	-0.89(1)			F4	-0.92(4)		
F5	-0.97(1)		F5	-1.02(2)			F5	-1.03(1)			F5	-0.99(1)			F5	-0.92(2)		

O1	-1.63(1)	O1	-1.61(1)	O1	-1.90(1)	O1	-1.80(1)	O1	-2.03(2)
O2	-1.82(1)	O2	-1.83(2)	O2	-1.99(2)	O2	-1.87(2)	O2	-2.1(1)
O3	-1.83(1)	O3	-1.87(2)	O3	-1.91(2)	O3	-1.91(2)	O3	-1.87(3)
O4	-1.87(1)	O4	-1.93(3)	O4	-1.86(2)	O4	-1.98(2)	O4	-2.0(1)
O5	-1.83(1)	O5	-1.92(2)	O5	-1.98(2)	O5	-1.91(2)	O5	-1.9(1)

[c] (R, b) parameters being for K^+-O (2.132, 0.37), K^+-F (1.992, 0.37), Rb^+-O (2.263, 0.37), Rb^+-F (2.16, 0.37), Cs^+-O (2.417, 0.37), Cs^+-F (2.33, 0.37), V^{3+}-O (1.743, 0.37), V^{3+}-F (1.702, 0.37), Fe^{3+}-O (1.759, 0.37), Fe^{3+}-F (1.679, 0.37), P^{5+}-O (1.617, 0.37), P^{5+}-F (1.54, 0.37)

Table 3. Results from Analysis of dc Magnetic Susceptibility Curves.

Compound	Exchange type, M-X-M J_1/K_B,K	g	χ_O, emu·mol^{-1}·Oe^{-1}	R^2	T_N,K	θ_{CW},K
$Rb(NH_4)_2V_4(PO_4)_2F_7(OH)_2$	-4.1(2)	1.76(3)	0.00003(1)	0.99997	-	-29(1)
$Cs_{1.3}(NH_4)_{1.7}V_4(PO_4)_2F_7(OH)_2$	-4.9(1)	1.76(3)	0.00002(1)	0.99997	-	-35(1)
$K(NH_4)_2Fe_4(PO_4)_2F_7(OH)_2$	-11.2(2)	1.99(2)	0.000006(2)	0.9962	5.5(2)	-277(1)
$Rb_{2.2}(NH_4)_{0.8}Fe_4(PO_4)_2F_7(OH)_2$	-12.5(1)	2.07(2)	0.000004(1)	0.99776	5.5(2)	-279(1)